Orbital magnetization in Sierpinski fractals

L. L. Lage,[1,*] Tarik P. Cysne,[1,†] and A. Latgé[1]

[1] *Instituto de Física, Universidade Federal Fluminense, Niterói, Av. Litorânea sn 24210-340, RJ-Brazil*

(Dated: October 22, 2025)

Orbital magnetization (OM) in Sierpinski carpet (SC) and triangle (ST) fractal is theoretically investigated by using Haldane model as a prototypical example. The OM calculation is performed following two distinct approaches; employing the definition and local markers formalism. Both methods coincides for all systems analyzed. For the SC, higher fractal generations create a dense set of edge states, resulting in a staircase profile, leading to oscillations in the magnetization as a function of the chemical potential. In contrast, the ST self-similarity produces distinct fractal-induced spectral gaps, which manifest as constant plateaus in the magnetization. The STs exhibit a pronounced sensitivity to edge terminations. Our results reveal how quantum confinement in fractal structures affects the electronic orbital angular momentum, pointing to possible pathways for exploring novel orbitronics in systems with complex geometries.

Introduction: Fractals are mathematical structures exhibiting self-similarity and non-integer dimensions [1]. Fractal structures are often found in nature and appear in contexts such as molecular chemistry [2, 3], biology [4, 5], and geography [6]. Of the many types of fractals, the Sierpinski fractals are some of the most studied. They are constructed from simple geometric shapes by iteratively removing specific regions, resulting in structures that exhibit self-similarity. For instance, the Sierpinski carpet (SC) is constructed through an iterative process of subdividing a solid square into a 3×3 grid of smaller congruent squares and removing the central square. This process is repeated recursively for each of the remaining eight squares, resulting in a structure composed of self-replicated solid squares. An analogous algorithm can be used to generate the Sierpinski triangle (ST) fractal.

In physics, electronic fractals have gained increasing attention in the last few years. With advances in the manipulation of matter at the nanoscale, the fabrication of nanostructured fractal patterns has become possible. Electronic fractal systems at the nanoscale have been constructed using various approaches, including bismuth nanostructures [7], surface-positioned molecules [8], and self-assembled molecular systems [9, 10], where electrons are constrained to move within fractal lattice geometries. The non-integer fractal dimension of this structure enables the emergence of many interesting and exotic phenomena. A remarkable example is the recent proposal in which electronic fractals can host topological phases even without the usual driving terms, such as spin-orbit coupling or magnetic fields, in the electronic Hamiltonian [11]. We also mention the possible loss of correlation between transport coefficients and topological invariants in certain electronic fractals, as pointed out by some numerical studies [12, 13]. Electronic fractals have also been known to exhibit particular charge localization [14, 15] and self-similarity in electronic responses [16–19]. Furthermore, fractal systems lack translational symmetry, making them interesting platforms for studying local topological aspects of matter [20–22]. In fact, real-space topology has been studied in fractal systems of both $\mathbb{Z}_2$ insulators and Chern insulators, including Sierpinski triangles [23–25] and Sierpinski carpets [26, 27]. Other types of topological phases in distinct fractal systems have also been explored [28–31].

Recently, electronic orbital angular momentum in condensed matter systems has piqued the interest of the scientific community. Its relevance to the equilibrium magnetization of nanostructured systems [32–34] and the development of novel approaches for generating nonequilibrium orbital currents [35, 36] and densities [37, 38] has given rise to the emerging field of orbitronics [39–41]. Understanding how magnetism manifests itself in fractal geometries remains an intriguing open question [42], especially in light of advances in nanoscale manipulation and the growing range of materials used in nanoscience. In particular, studying the orbital contribution to the magnetization of fractal nanostructures is appealing, given the strong dependence of the electronic spectrum on the specific fractal geometry. To explore theses effects, we study the Haldane model, a paradigmatic example exhibiting orbital magnetization, on two different Sierpinski fractal architectures. Firstly, we present results for the Sierpinski carpet, focusing on the evolution of equilibrium orbital magnetization of the system, with fractal generation of the Sierpinski carpets. A subsequent analysis for Sierpinski triangles highlights the emergence of fractal-induced energy gaps and the crucial role of edge termination geometry.

Model and Methods: In our study, we consider electrons described by the Haldane Hamiltonianon, which can be

* lucaslage@id.uff.br
† tarik.cysne@gmail.com

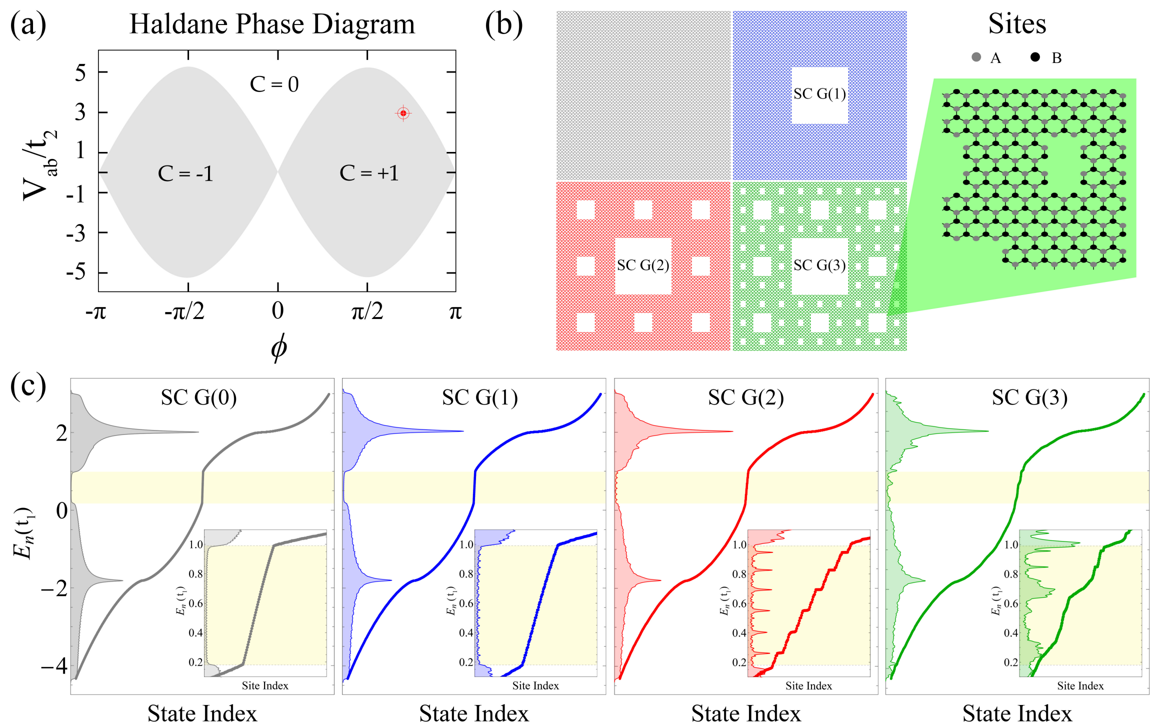

FIG. 1. (a) Topological phase diagram of the 2D Haldane model. The red mark indicates the parameters used in this work. (b) Four generations of the Sierpinski carpet (SC), with a magnified view of the underlying honeycomb lattice. (c) Energy spectra and density of states for SC G(0-4). The inset shows in-gap states from the topological phase. Yellow shading indicates the Haldane bulk gap for parameters $V_{ab}/t_2 = 3.0$, $\phi = 0.7\pi$ [red mark in (a)].

written in real space as,

$$\mathcal{H}_{\rm H} \;=\; t_1 \sum_{\langle \mathbf{i},\mathbf{j}\rangle} c_{\mathbf{i}}^\dagger c_{\mathbf{j}} + V_{\rm ab} \sum_{\mathbf{i}} \tau_{\mathbf{i}} c_{\mathbf{i}}^\dagger c_{\mathbf{i}} + t_2 \sum_{\langle\langle \mathbf{i},\mathbf{j}\rangle\rangle} e^{i\nu_{\mathbf{ij}}\phi} c_{\mathbf{i}}^\dagger c_{\mathbf{j}} \;+\; \text{H.c.} \;, \tag{1}$$

where t_1 is the intensity of hopping between nearest-neighbor sites $\langle \mathbf{i},\mathbf{j}\rangle$ in the underlying honeycomb structure. $V_{\rm ab}$ is the intensity of sublattice potential with, $\tau_{\mathbf{i}} = +1(-1)$ for the sites at sublattice $A(B)$. The strength coupling t_2 between the next-nearest-neighbor sites ($\langle\langle \mathbf{i},\mathbf{j}\rangle\rangle$) captures the effect of the staggered flux ϕ introduced in the model [43]. In this term, $\nu_{\mathbf{ij}} = +1(-1)$ for clock (counter clock)-wise orientations of hoppings. The illustrative topological phase diagram of this model in the 2D bulk system is shown in Figure 1 (a). It is composed of two topologically non-trivial phases with Chern numbers $C = \pm 1$ and a topologically trivial phase with zero Chern number ($C = 0$). All calculations were performed adopting $t_2 = t_1/3$, $V_{ab}/t_2 = 3.0$, and $\phi = 0.7\pi$.

The Haldane model breaks the time-reversal symmetry, enabling equilibrium orbital magnetization. As a simple electronic model, it has served as a paradigm for exploring new aspects of this phenomenon [44–46]. Here, we consider the Haldane model in fractal geometries and examine the impact of fractality on orbital magnetization.

The magnetization arising from electronic orbital angular momentum can be defined as:

$$M = -\frac{e}{2cA} \sum_{E_n<\mu} \langle \phi_n | \, \mathbf{r} \times \mathbf{v} \, | \phi_n \rangle \, , \tag{2}$$

where, A is the area of the sample, $\mathbf{v} = -\frac{i}{\hbar}[\mathbf{r}, \mathcal{H}]$ is the velocity operator, and $|\phi_n\rangle$ are eigenstates of the real-space Hamiltonian $\mathcal{H}$ with eigenenergies E_n. The summation in Eq. (2) runs over all the occupied states, $E_n < \mu$, where μ is the chemical potential. The orbital magnetization can be written as $M = -\frac{ie}{2\hbar cA} \sum_{E_n<\mu} (\langle \phi_n | x\mathcal{H}y | \phi_n\rangle - \langle \phi_n | y\mathcal{H}x | \phi_n\rangle)$. Bianco and Resta showed in Ref. [44] that Eq. (2) can be expressed as a sum over a local quantity in real space. By writing the ground state projector, $\mathcal{P} = \sum_{E_n<\mu} |\phi_n\rangle \langle \phi_n|$, and its complement $\mathcal{Q} = \mathbb{1} - \mathcal{P}$, one can define a local mathematical object, i.e., a marker, that plays the role

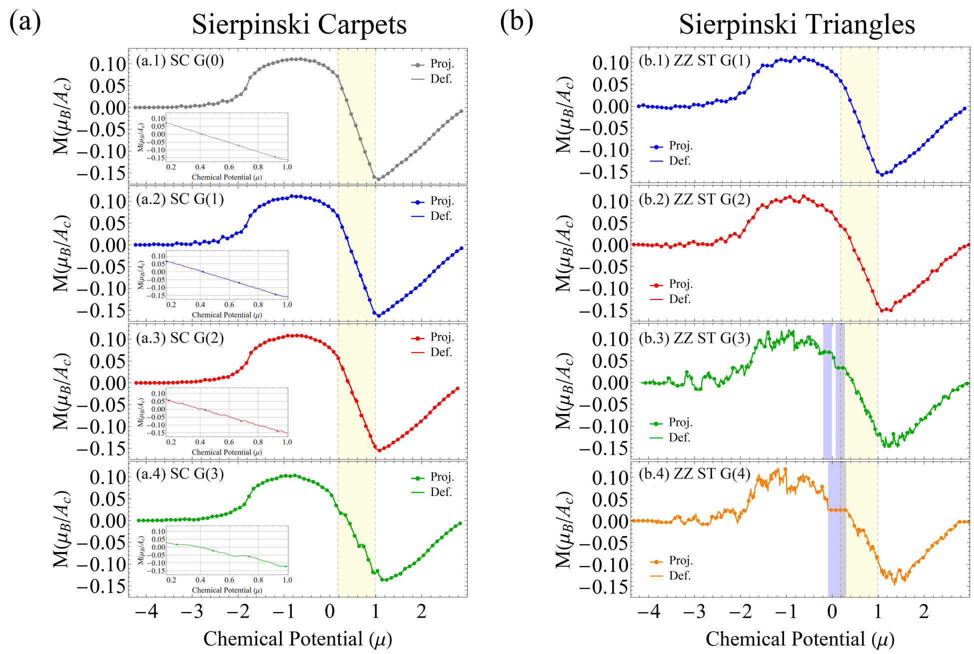

FIG. 2. (a) Orbital magnetization vs. chemical potential in the Haldane model for Sierpinski carpet generations G(0−3) (a.1−4) and also for (b) Sierpinski triangle generations G(1−4) (b.1−4). Solid lines represent the results obtained using the definition of orbital magnetization [Eq. (2)], while circles represent the results obtained from the local markers formulation. The shaded yellow region corresponds to 2D bulk gap in the Haldane model with $V_{ab}/t_2 = 3.0$, $\phi = 0.7\pi$. Blue areas in panels (b.1−4) mark fractal-induced gaps in ZZ ST. The insets in panels (a.1−4) show magnified views of orbital magnetization in the 2D bulk gap region for SC.

of an orbital magnetic moment density:

$$
\begin{aligned}
m(\mathbf{r}) &= m_{\rm LC}(\mathbf{r}) + m_{\rm IC}(\mathbf{r}) + m_{\rm BC}(\mathbf{r}), && (3)\\
m_{\rm LC}(\mathbf{r}) &= \frac{e}{\hbar c}\mathrm{Im}\,\langle \mathbf{r}|\,\mathcal{P}x\mathcal{Q}\mathcal{H}\mathcal{Q}y\mathcal{P}\,|\mathbf{r}\rangle\,, && (4)\\
m_{\rm IC}(\mathbf{r}) &= -\frac{e}{\hbar c}\mathrm{Im}\,\langle \mathbf{r}|\,\mathcal{Q}x\mathcal{P}\mathcal{H}\mathcal{P}y\mathcal{Q}\,|\mathbf{r}\rangle\,, && (5)\\
m_{\rm BC}(\mathbf{r}) &= \mu\frac{e}{2\pi\hbar c}\mathfrak{C}(\mathbf{r}). && (6)\\
\mathfrak{C}(\mathbf{r}) &= 4\pi\mathrm{Im}\,\langle \mathbf{r}|\,\mathcal{Q}x\mathcal{P}y\mathcal{Q}\,|\mathbf{r}\rangle && (7)
\end{aligned}
$$

It is worth noting that, despite this interpretation of the markers, only the macroscopic average of $m(\mathbf{r})$ has physical significance, as discussed in Ref. [47]. In Ref. [48], it was shown that the orbital magnetization obtained from local markers coincides with that obtained from the definition of Eq.(2), provided the macroscopic average is taken over the entire sample area, including both bulk and edge regions.

$$
M = \frac{1}{A}\int_A m(\mathbf{r})d\mathbf{r}\ . \qquad (8)
$$

This agreement holds even for small systems subjected to open boundary conditions (OBC). In each fractal generation, the integration area used in the average is given by $A = N_{\rm c}A_{\rm c}$, where the number of elementary cells in the structure, N_c, is half the number of sites and $A_{\rm c}$ is the area of one cell. To calculate the orbital magnetization of fractal systems, we shall use both expressions [Eqs. (2) and (8)] to test this coincidence in the more intricate fractal geometry.

Sierpinski Carpet: The Sierpinski carpet (SC) is geometrically constructed by systematically inserting vacancies inside a bidimensional region, creating different generations $G(n)$. By increasing the number of vacancies the SC dimension assumes a fractional value of $D = log(8)/log(3) \approx 1.89$ independently of the generation. Adopting a honeycomb lattice mesh inside the carpet, the external lengths are fixed between the generations G(0−3) and the corresponding number of lattice sites are $N_i = 11772,\ 10512,\ 9456,\ 8688$ sites ($i = 0, ..., 3$), respectively, as shown in gray, blue, red and green in Fig. 1 (b). Both external and internal edges of the carpet are formed by sequences of armchair and zigzag contours. The resulting energy spectrum of SCs G(0−3) are exhibited in panel (c) of Fig. 1 following the previously described colored pattern. The adopting parametrization were adjusted to match with a topological phase ($C = \pm 1$) inside the 2D bulk Haldane diagram with $V_{ab}/t_2 = 3.0$ and $\phi = 0.7\pi$, which describes the anomalous quantum Hall effect [see Fig. 1 (a)]. As expected from the bulk results [43], in this phase the finite system subjected to OBC has protected edge states inside the bulk energy gap region. Such states develop a staircase profile as the generation of the fractal is increased [30, 49], which implies in emergent peaks in the total density of states (DOS) for this region, as shown in Fig. 1 (c). In fractals

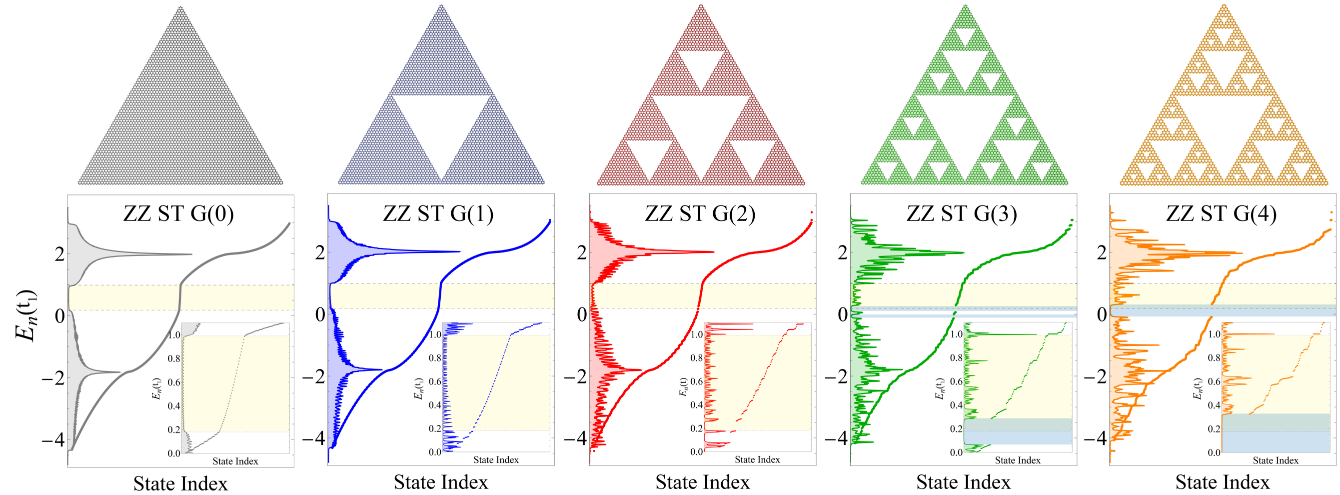

FIG. 3. (a) Illustration of five generations of the Sierpinski Triangle with zigzag edges [ZZ ST G(0−4)] considered in our calculations. (b) Energy spectra with the corresponding density of states for ZZ ST G(0−4). The inset magnifies the region of in-gap states, which appear in the system subjected to open boundary conditions when parameters are adjusted to reach the topological phase of the model. The yellow shaded region represents the band gap of the 2D bulk Haldane model, obtained with the same coupling constants ($V_{ab}/t_2 = 3.0$ and $\phi = 0.7\pi$) used in our calculations within the fractal geometry (red mark in Fig. 1 (a)). The blue shaded strips correspond to the fractal induced energy gaps opened in the energy spectra of ZZ ST.

this is characterized by emergent edge states occurring in external and internal edges of the system, the later being related with the fractal generation. For the proposed systems, this pattern results from a competition between the lattice parameters and the fractal order, emerging as the vacancies are inserted, as seen for different types of models and fractals [30].

In Fig. 2 (a.1−4) we present the calculated orbital magnetization, M, as a function of the chemical potential, μ, for the first four generations of the Sierpinski carpets, i.e. G(0−3). In each panel, the results of the two distinct computational methods are shown to be in perfect matching; the solid lines represent the magnetization calculated from its fundamental definition (Eq. 2), while the circles are obtained from the local marker with projectors formulation (Eqs. 3 and 8). The shaded yellow region highlights the energy range of the bulk topological gap of the 2D Haldane model. For the initial G(0) generation in panel (a.1), the magnetization exhibits a linear trend within this gap, which is a signature of a finite bulk Chern number. It should be noted that the result in Fig. 2 (a.1), obtained here from the real-space calculation for a flake with OBC [SC G(0)], coincides with those obtained from the **k**-space calculation in 2D bulk for the same set of parameters [46]. As the fractal generation increases from G(1) to G(3) significant fluctuations appears in panels (a.2 − 4) and become more frequent. This behavior is a direct consequence of the fractal nature of the system, reflecting the "staircase" profile of the several internal and external edge states that emerge in the energy spectrum, as highlighted in the magnified view of this energy region in the insets of Fig. 2 (a).

Sierpinski Triangle: Similarly to the Sierpinski carpet, the Sierpinski triangle (ST) is constructed, exhibiting a fractional dimension of $D = \log(3)/\log(2) \approx 1.58$. Given the C_3 rotational symmetry of the triangular structures, by adopting a honeycomb lattice, we have two distinct edge configurations for the full Sierpinski triangle; zigzag (ZZ ST) and armchair (AC ST). As previously reported [16], the electronic properties of ZZ and AC STs are intrinsically distinct. The high sensitivity of ST quantum states, related to its edge configurations, comes directly from the fundamental physics of the quantum confinement in a honeycomb lattice.

We start exploring the ZZ edge configurations, whose generations G(0−4) with the number of sites N_{0-4} = 5773, 5030, 3924, 3125, 2450 are depicted at the top of Fig. 3, in gray, blue, red, green, and orange, respectively, adopting the same parameters within Haldane model of the SCs.

Unlike SCs, the inherent symmetry of STs, promotes the emergence of additional fractal gaps within the energy spectrum, which the principals are highlighted by blue shaded areas in the lower panel of Fig. 3. Within the yellow shaded region of the same figure, a distinct staircase profile is also observed for some of the edge states residing inside the Haldane bulk gap. The states are separated by such induced gaps in both fundamental/excited and Fermi energies. Because of the difference in crystal symmetry compared to the Sierpinski carpets, the electronic properties of the Sierpinski triangle are modified by changing the edge termination, as seen in the results for the zigzag and armchair configurations in Fig. 2(b) and Fig. 4, respectively. Fig. 4

summarizes the electronic and magnetic properties of a 6th generation Sierpinski triangle with armchair edges (AC ST G(6)), as illustrated by its lattice structure in panel (a). The corresponding energy spectrum is presented in panel (b), where the yellow shaded region indicates the Haldane bulk gap, and the blue shaded regions mark the additional energy gaps that arise from the fractal geometry. Panel (c) demonstrates the direct correspondence between the gaped regions of the spectrum and the orbital magnetization. For both types of ST, the fractal-induced gaps produce constant orbital magnetization for different values of the chemical potential, including those within the energy region corresponding to the Haldane 2D bulk gap.

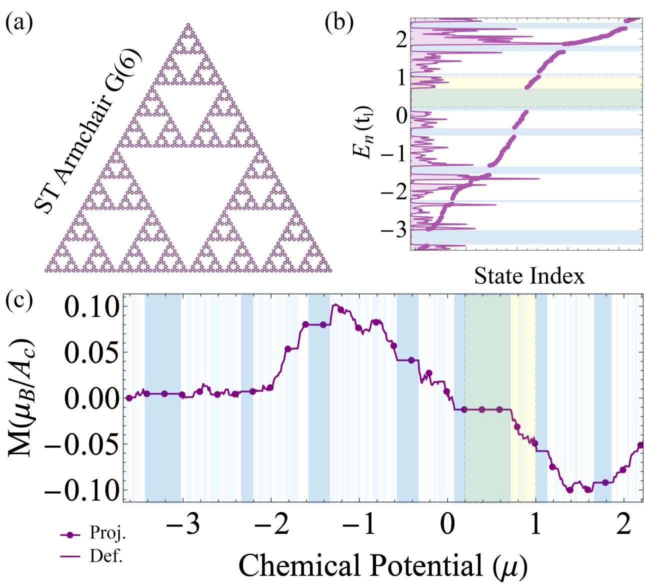

FIG. 4. (a) Sierpinski triangle, G(6), armchair edges [AC ST G(6)]. (b) Energy spectrum and density of states for the Haldane model ($V_{ab}/t_2 = 3.0$, $\phi = 0.7\pi$). Yellow shading: bulk band gap; blue: fractal-induced gaps. (c) Orbital magnetization versus chemical potential in circles and lines corresponding with definition (Eq. 2), and local markers formulation, respectively, with blue areas indicating energy gaps.

The more significant fractal-induced gaps and corresponding plateaus in orbital magnetization for both ZZ ST and AC ST are highlighted in blue shaded rectangles in Figure 2 (b) and Fig. 4 (c), respectively. Interestingly, for ST AC G(6), a large fractal gap overlaps with much of the 2D Haldane bulk gap, producing a wide plateau in the graph of orbital magnetization versus chemical potential. For both types of ST, the results obtained using the primary definition of orbital magnetization (Eq. 2), denoted by a continuous line, and those obtained from the local markers formulation (Eq. 3 and 8), denoted by circles, coincide. The local markers approach provides a transparent picture of the emergence of plateaus in orbital magnetization produced by fractal gaps. When the chemical potential μ passes through an energy range with no electronic states (fractal gap), the ground-state projector $\mathcal{P}$ remains invariant, and, since the whole-sample average of $\mathfrak{C}(\mathbf{r})$ in a system with OBC $[\int_A d\mathbf{r}\mathfrak{C}(\mathbf{r})]$ is enforced to vanish [21, 48], no change in orbital magnetization occurs. The analysis of the local Chern marker in distinct fractal-induced gaps for ST ZZ is presented in the supplementary material.

These results illustrate the direct impact of the fractal geometry on the orbital magnetization. As the fractal generation increases, the orbital magnetization curve develops a more intricate structure, reflecting the emergence of a more complex hierarchy of energy gaps in the electronic spectrum.

Final Remarks: The emergence of new fractal-induced gaps is a direct consequence of the ST geometry. Its iterative construction creates a self-organized hierarchy of boundaries, leading to quantum confinement that quantizes the electronic energy levels. The triangular geometry ensures each spatial side composed by a single, pure edge type either zigzag (ZZ) or armchair (AC), whose intrinsic properties dominate the electronic behavior. Consequently, switching the boundary type drastically modifies the energy spectra and orbital magnetization, which exhibit distinct plateaus within these fractal-induced gaps. In contrast to SCs fractals, which develop a dense, staircase-like spectrum and growing oscillations in orbital magnetization, the STs emergent gaps promote constant orbital magnetization plateaus. This shows how quantum confinement in fractal geometry can be used to explore novel properties of electronic orbital angular momentum, offering an interesting perspective in the emerging field of orbitronics [39]. Proposals and experimental realizations of fractal geometry are available for different types of physical systems [7, 8, 29, 50–52]. Furthermore, the Haldane model, used here as a prototypical example, can be realized in different contexts, such as magneto-optical lattices [53], ultracold fermion lattices [54], Fe-based insulators [55], and topoelectrical circuits [56], opening a perspective to study the phenomenology discussed here.

Acknowledgments: The authors would like to thank the INCT de Nanomateriais de Carbono for providing support on the computational infrastructure. LLL thanks the CNPq scholarship. TPC acknowledges CNPq (Grant No. 305647/2024-5). AL thanks FAPERJ (Grant E-26/200.569/2023).

[1] B. B. Mandelbrot, *The fractal geometry of nature* (1983).
[2] S. Sadegh, J. L. Higgins, P. C. Mannion, M. M. Tamkun, and D. Krapf, Plasma membrane is compartmentalized by a self-similar cortical actin meshwork, Phys. Rev. X

7, 011031 (2017).

[3] F. L. Sendker, Y. K. Lo, T. Heimerl, S. Bohn, L. J. Persson, C.-N. Mais, W. Sadowska, N. Paczia, E. Nußbaum, M. del Carmen Sánchez Olmos, K. Forchhammer, D. Schindler, T. J. Erb, J. L. P. Benesch, E. G. Marklund, G. Bange, J. M. Schuller, and G. K. A. Hochberg, Emergence of fractal geometries in the evolution of a metabolic enzyme, Nature **628**, 894–900 (2024).

[4] T. Smith, W. Marks, G. Lange, W. Sheriff, and E. Neale, A fractal analysis of cell images, Journal of Neuroscience Methods **27**, 173 (1989).

[5] Y. Wang, K. Leiberg, N. Kindred, C. R. Madan, C. Poirier, C. I. Petkov, P. N. Taylor, and B. Mota, Neuro-evolutionary evidence for a universal fractal primate brain shape, eLife **12**, RP92080 (2024).

[6] B. Jiang and S. A. Brandt, A fractal perspective on scale in geography, ISPRS International Journal of Geo-Information **5**, 10.3390/ijgi5060095 (2016).

[7] R. Canyellas, C. Liu, R. Arouca, L. Eek, G. Wang, Y. Yin, D. Guan, Y. Li, S. Wang, H. Zheng, C. Liu, J. Jia, and C. Morais Smith, Topological edge and corner states in bismuth fractal nanostructures, Nature Physics **20**, 1421–1428 (2024).

[8] S. N. Kempkes, M. R. Slot, S. E. Freeney, S. J. M. Zevenhuizen, D. Vanmaekelbergh, I. Swart, and C. M. Smith, Design and characterization of electrons in a fractal geometry, Nature Physics **15**, 127–131 (2018).

[9] G. R. Newkome, P. Wang, C. N. Moorefield, T. J. Cho, P. P. Mohapatra, S. Li, S.-H. Hwang, O. Lukoyanova, L. Echegoyen, J. A. Palagallo, V. Iancu, and S.-W. Hla, Nanoassembly of a fractal polymer: A molecular "sierpinski hexagonal gasket", Science **312**, 1782–1785 (2006).

[10] J. Shang, Y. Wang, M. Chen, J. Dai, X. Zhou, J. Kuttner, G. Hilt, X. Shao, J. M. Gottfried, and K. Wu, Assembling molecular sierpiński triangle fractals, Nature Chemistry **7**, 389–393 (2015).

[11] L. Eek, Z. F. Osseweijer, and C. Morais Smith, Fractality-induced topology, Phys. Rev. Lett. **134**, 246601 (2025).

[12] A. A. Iliasov, M. I. Katsnelson, and S. Yuan, Hall conductivity of a sierpiński carpet, Phys. Rev. B **101**, 045413 (2020).

[13] M. Fremling, M. van Hooft, C. M. Smith, and L. Fritz, Existence of robust edge currents in sierpiński fractals, Phys. Rev. Res. **2**, 013044 (2020).

[14] L. L. Lage and A. Latgé, Quasi-one-dimensional carbon-based fractal lattices, Frontiers in Carbon **2**, 1 (2023).

[15] S. Fischer, M. van Hooft, T. van der Meijden, C. M. Smith, L. Fritz, and M. Fremling, Robustness of chiral edge modes in fractal-like lattices below two dimensions: A case study, Phys. Rev. Res. **3**, 043103 (2021).

[16] T. G. Pedersen, Graphene fractals: Energy gap and spin polarization, Phys. Rev. B **101**, 235427 (2020).

[17] A. Agarwala, Seeking topological phases in fractals, in *Excursions in Ill-Condensed Quantum Matter: From Amorphous Topological Insulators to Fractional Spins* (Springer International Publishing, Cham, 2019) pp. 81–92.

[18] L. L. Lage and A. Latgé, Electronic fractal patterns in building sierpinski-triangle molecular systems, Phys. Chem. Chem. Phys. **24**, 19576 (2022).

[19] B. Pal and K. Saha, Flat bands in fractal-like geometry, Phys. Rev. B **97**, 195101 (2018).

[20] S. A. Sousa-Júnior, M. V. d. S. Ferraz, J. P. de Lima, and T. P. Cysne, Topological characterization of modified kane-mele-rashba models via local spin chern marker, Phys. Rev. B **111**, 035411 (2025).

[21] R. Bianco and R. Resta, Mapping topological order in coordinate space, Phys. Rev. B **84**, 241106 (2011).

[22] N. Baù and A. Marrazzo, Theory of local $\mathbb{Z}_2$ topological markers for finite and periodic two-dimensional systems, Phys. Rev. B **110**, 054203 (2024).

[23] Z. F. Osseweijer, L. Eek, A. Moustaj, M. Fremling, and C. Morais Smith, Haldane model on the sierpiński gasket, Phys. Rev. B , 245405 (2024).

[24] M. Brzezińska, A. M. Cook, and T. Neupert, Topology in the sierpiński-hofstadter problem, Phys. Rev. B **98**, 205116 (2018).

[25] S. Pai and A. Prem, Topological states on fractal lattices, Phys. Rev. B **100**, 155135 (2019).

[26] A. Rojo-Francàs, P. Pansari, U. Bhattacharya, B. Juliá-Díaz, and T. Grass, Anomalous quantum transport in fractal lattices, Communications Physics **7**, 259 (2024), received: 14 February 2024; Accepted: 14 July 2024; Published: 02 August 2024.

[27] L. L. Lage, A. B. Félix, S A Sousa-Júnior, A. Latgé, and T. P. Cysne, Topological phases in fractals: Local spin chern marker in the kane-mele-rashba model on the sierpinski carpet, Phys. Rev. B , 245418 (2025).

[28] S. Manna and B. Roy, Inner skin effects on non-hermitian topological fractals, Communications Physics **6**, 10.1038/s42005-023-01130-2 (2023).

[29] X. Chen and R. Yu, Realization of fractal aubry-andré-harper models in electronic circuits, Phys. Rev. B **111**, 235104 (2025).

[30] L. L. Lage, N. C. Rappe, and A. Latgé, Corner and edge states in topological sierpinski carpet systems, Jour. Phys. Cond. Matt. , 025303 (2025).

[31] W. Cao, X. Qin, W. Zhang, X. Zhou, and X. Zhang, Topological fractal braiding of non-hermitian bands, Communications Physics **8**, 391 (2025).

[32] C. L. Tschirhart, M. Serlin, H. Polshyn, A. Shragai, Z. Xia, J. Zhu, Y. Zhang, K. Watanabe, T. Taniguchi, M. E. Huber, and A. F. Young, Imaging orbital ferromagnetism in a moiré chern insulator, Science **372**, 1323–1327 (2021).

[33] S. Peredkov, M. Neeb, W. Eberhardt, J. Meyer, M. Tombers, H. Kampschulte, and G. Niedner-Schatteburg, Spin and orbital magnetic moments of free nanoparticles, Phys. Rev. Lett. **107**, 233401 (2011).

[34] X. Liu, C. Wang, X.-W. Zhang, T. Cao, and D. Xiao, Orbital magnetization in correlated states of twisted bilayer transition metal dichalcogenides (2025), arXiv:2510.01727 [cond-mat.mes-hall].

[35] T. P. Cysne, M. Costa, L. M. Canonico, M. B. Nardelli, R. B. Muniz, and T. G. Rappoport, Disentangling orbital and valley hall effects in bilayers of transition metal dichalcogenides, Phys. Rev. Lett. **126**, 056601 (2021).

[36] D. Go, D. Jo, C. Kim, and H.-W. Lee, Intrinsic spin and orbital hall effects from orbital texture, Phys. Rev. Lett. **121**, 086602 (2018).

[37] T. P. Cysne, F. S. M. Guimarães, L. M. Canonico, M. Costa, T. G. Rappoport, and R. B. Muniz, Orbital magnetoelectric effect in nanoribbons of transition metal dichalcogenides, Phys. Rev. B **107**, 115402 (2023).

[38] A. Johansson, Theory of spin and orbital edelstein effects, Journal of Physics: Condensed Matter **36**, 423002 (2024).

[39] T. P. Cysne, L. M. Canonico, M. Costa, R. B. Muniz, and T. G. Rappoport, Orbitronics in two-dimensional materials, npj Spintronics **3**, 10.1038/s44306-025-00103-1 (2025).

[40] D. Jo, D. Go, G.-M. Choi, and H.-W. Lee, Spintronics meets orbitronics: Emergence of orbital angular momentum in solids, npj Spintronics **2**, 10.1038/s44306-024-00023-6 (2024).

[41] R. B. Atencia, A. Agarwal, and D. Culcer, Orbital angular momentum of bloch electrons: equilibrium formulation, magneto-electric phenomena, and the orbital hall effect, Advances in Physics: X **9**, 2371972 (2024), https://doi.org/10.1080/23746149.2024.2371972.

[42] M. Conte, V. Zampronio, M. Röntgen, and C. M. Smith, The fractal-lattice hubbard model, Quantum **8**, 1469 (2024).

[43] F. D. M. Haldane, Model for a quantum hall effect without landau levels: Condensed-matter realization of the "parity anomaly"', Phys. Rev. Lett. **61**, 2015 (1988).

[44] R. Bianco and R. Resta, Orbital magnetization as a local property, Phys. Rev. Lett. **110**, 087202 (2013).

[45] T. Thonhauser, D. Ceresoli, D. Vanderbilt, and R. Resta, Orbital magnetization in periodic insulators, Phys. Rev. Lett. **95**, 137205 (2005).

[46] D. Ceresoli, T. Thonhauser, D. Vanderbilt, and R. Resta, Orbital magnetization in crystalline solids: Multi-band insulators, chern insulators, and metals, Phys. Rev. B **74**, 024408 (2006).

[47] D. Seleznev and D. Vanderbilt, Towards a theory of surface orbital magnetization, Phys. Rev. B **107**, 115102 (2023).

[48] S.-S. Wang, Y. Yu, J.-H. Guan, Y.-M. Dai, H.-H. Wang, and Y.-Y. Zhang, Boundary effects on orbital magnetization for a bilayer system with different chern numbers, Phys. Rev. B **106**, 075136 (2022).

[49] J. Li, Y. Sun, Q. Mo, Z. Ruan, and Z. Yang, Fractality-induced topological phase squeezing and devil's staircase, Phys. Rev. Res. **5**, 023189 (2023).

[50] J. He, H. Jia, H. Chen, T. Wang, S. Liu, J. Cao, Z. Gao, C. Shang, and T. J. Cui, Mode engineering in reconfigurable fractal topological circuits, Phys. Rev. B **109**, 235406 (2024).

[51] C. Li, X. Zhang, N. Li, Y. Wang, J. Yang, G. Gu, Y. Zhang, S. Hou, L. Peng, K. Wu, D. Nieckarz, P. Szabelski, H. Tang, and Y. Wang, Construction of sierpiński triangles up to the fifth order, Journal of the American Chemical Society **139**, 13749 (2017), pMID: 28885024, https://doi.org/10.1021/jacs.7b05720.

[52] N. E. Myerson-Jain, S. Yan, D. Weld, and C. Xu, Construction of fractal order and phase transition with rydberg atoms, Phys. Rev. Lett. **128**, 017601 (2022).

[53] M. J. Ablowitz and J. T. Cole, Generalized haldane model in a magneto-optical honeycomb lattice, Phys. Rev. A **109**, 033503 (2024).

[54] G. Jotzu, M. Messer, R. Desbuquois, M. Lebrat, T. Uehlinger, D. Greif, and T. Esslinger, Experimental realization of the topological Haldane model with ultracold fermions, Nature **515**, 237 (2014).

[55] H.-S. Kim and H.-Y. Kee, Realizing Haldane model in Fe-based honeycomb ferromagnetic insulators, npj Quantum Materials **2**, 20 (2017).

[56] R. Haenel, T. Branch, and M. Franz, Chern insulators for electromagnetic waves in electrical circuit networks, Phys. Rev. B **99**, 235110 (2019).